

Western Pacific modulation of large phytoplankton blooms in the central and eastern equatorial Pacific

John P. Ryan,¹ Iwao Ueki,² Yi Chao,³ Hongchun Zhang,^{3,4} Paulo S. Polito,⁵ and Francisco P. Chavez¹

Received 5 August 2005; revised 26 January 2006; accepted 9 February 2006; published 7 June 2006.

[1] Satellite observations show that large-scale phytoplankton blooms (increases in chlorophyll) occurred in the equatorial Pacific in 1998, 2003, and 2005, following termination of the three most recent El Niño events. The occurrence of blooms following successive El Niño events cannot be explained by local enhancement of vertical nutrient flux, as evidenced by observations of equatorial winds, thermocline depth, and the depth and strength of the Equatorial Undercurrent (EUC, which supplies the limiting nutrient iron to the euphotic zone). However, near the peak of each El Niño event (late in 1997, 2002, and 2004), while the thermocline of the western equatorial Pacific was anomalously shallow, the flow of the New Guinea Coastal Undercurrent (NGCUC, which is the primary source of iron-enriched waters to the EUC) intensified, and its core shoaled from >200 m to ~100 m depth. Analysis of NGCUC variability using a high-resolution, terrain-following three-dimensional ocean circulation model simulation indicates that as the NGCUC shoals and intensifies, it develops meanders and eddies that augment coupling of the New Guinea shelf and upper slope to the EUC. We hypothesize that these changes in NGCUC circulation during El Niño enhance iron transport from the New Guinea margin into the EUC and thereby trigger large-scale blooms when iron-enriched waters subsequently reach the euphotic zone along the equator. The threefold to fourfold chlorophyll increases over large regions, up to $\sim 5 \times 10^5 \text{ km}^2$, must have profound impacts on the equatorial ecosystem and biogeochemical cycles.

Citation: Ryan, J. P., I. Ueki, Y. Chao, H. Zhang, P. S. Polito, and F. P. Chavez (2006), Western Pacific modulation of large phytoplankton blooms in the central and eastern equatorial Pacific, *J. Geophys. Res.*, *111*, G02013, doi:10.1029/2005JG000084.

1. Introduction

[2] The equatorial Pacific upwelling spans one quarter of the global equatorial circumference and is responsible for one quarter of the new production in the global ocean [Chavez and Toggweiler, 1995]. The signature of upwelling is evident in climatological sea surface temperature as a cold tongue along the equator extending from the eastern margin to the western Pacific warm pool (Figure 1a). Primary productivity in the equatorial Pacific is enhanced by upwelling, however macronutrients are not fully utilized by phytoplankton, presumably due to iron limitation [Martin *et al.*, 1991]. Limitation of phytoplankton growth by low concentrations of iron in surface waters of the equatorial

Pacific is supported by phytoplankton bottle incubation experiments [Martin *et al.*, 1991], by observations of natural conditions [Barber and Chavez, 1991; Coale *et al.*, 1996a; Gordon *et al.*, 1997; Landry *et al.*, 1997], and by experimental large-scale iron fertilization [Martin *et al.*, 1994; Coale *et al.*, 1996b; Behrenfeld *et al.*, 1996]. Iron limitation of productivity limits photosynthetic uptake of CO₂ by phytoplankton and contributes to the equatorial Pacific being the largest natural source of CO₂ to the atmosphere. The 0.5–1 Pg (10¹⁵ g) of carbon outgassed as CO₂ annually [Chavez *et al.*, 1999] is equivalent to 8–16% of the annual release by fossil fuel burning [Intergovernmental Panel on Climate Change, 2001].

[3] Iron supply to the euphotic zone of the equatorial Pacific is dominated by upward flux from the Equatorial Undercurrent (EUC), which contains elevated concentrations of dissolved and particulate iron [Coale *et al.*, 1996a; Gordon *et al.*, 1997]. The EUC flows eastward across the Pacific, shoaling to the east in parallel with the thermocline (Figure 1b). Vertical displacement of the thermocline and EUC changes the supply of iron and macronutrients to the euphotic zone. Thermocline depth in the equatorial Pacific is strongly influenced by the El Niño/Southern Oscillation (ENSO), which modulates wind patterns, ocean circulation, and water mass distributions of the tropical Pacific [Philander,

¹Monterey Bay Aquarium Research Institute, Moss Landing, California, USA.

²Japan Agency for Marine-Earth Science and Technology, Yokosuka, Japan.

³Jet Propulsion Laboratory, California Institute of Technology, Pasadena, California, USA.

⁴Raytheon Information Technology and Scientific Services, Pasadena, California, USA.

⁵Instituto Oceanográfico da Universidade de São Paulo, Sao Paulo, Brazil.

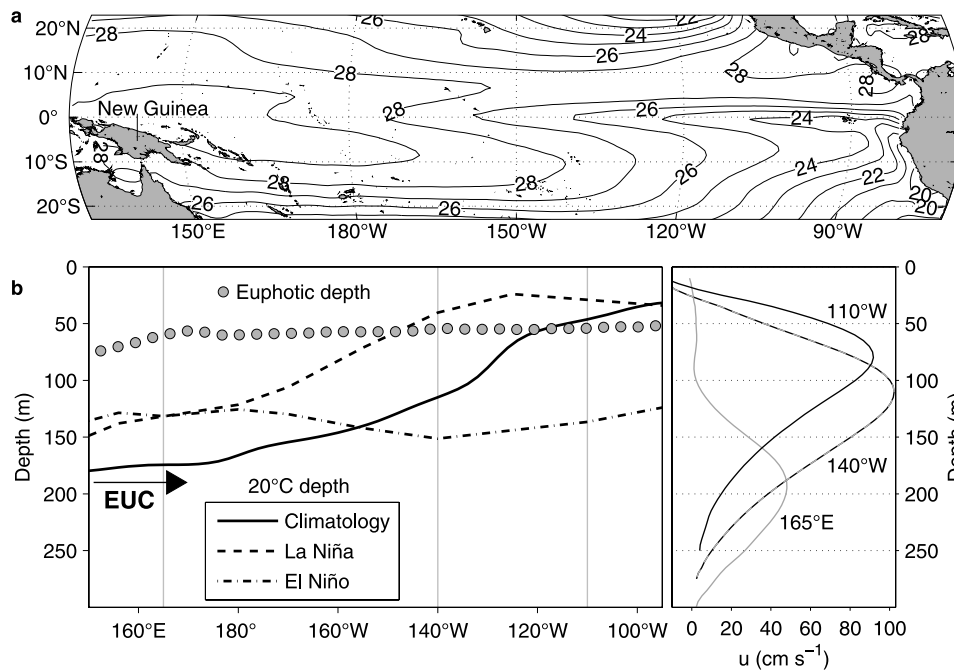


Figure 1. Conceptual model. (a) Climatological sea surface temperature (SST) in the tropical Pacific, illustrating the equatorial upwelling cold tongue in the east and warm pool in the west. (b) Vertical section along the equator, illustrating thermocline and EUC shoaling from west to east that is present under normal and La Niña conditions but is reduced or eliminated during El Niño conditions. ENSO modulation of thermocline depth influences nutrient supply to the euphotic zone. Euphotic depth was defined from mean satellite-derived chlorophyll concentrations and an empirical relationship between measured in situ surface chlorophyll concentrations and euphotic depth (1% light level) in this region (MBARI data archive). Depth of the 20°C isotherm is defined from the Tropical Atmosphere Ocean (TAO) mooring array data; the El Niño data are from October–December 1997, and the La Niña data are from June–August 1998. Mean profiles of zonal velocity (u) at 165°E, 140°W, and 110°W represent zonal variation in the depth and strength of the eastward flowing Equatorial Undercurrent (EUC).

1990; McPhaden, 1999]. These physical changes have significant biological consequences. During El Niño, depression of the thermocline in the eastern equatorial Pacific moves nutrient source waters away from the euphotic zone (Figure 1b), reducing nutrient supply and phytoplankton productivity [Chavez *et al.*, 1999; Strutton and Chavez, 2000]. During La Niña, elevation of the thermocline in the eastern equatorial Pacific moves nutrient source waters toward the euphotic zone (Figure 1b), enhancing nutrient supply and phytoplankton productivity along the equator.

[4] The exceptionally strong 1997–1998 ENSO cycle was the first thoroughly observed by satellite remote sensing of ocean surface spectral reflectance (ocean color), a method enabling estimates of chlorophyll concentration. Following dramatic decreases in primary production during the El Niño, a massive bloom occurred in the central and eastern equatorial Pacific during the 1998 transition to La Niña [Chavez *et al.*, 1999]. A model analysis indicated that the observed increases in chlorophyll concentrations could be explained by enhanced iron flux resulting from the anomalously shallow thermocline in the central equatorial Pacific [Chavez *et al.*, 1999]. Diverse physical phenomena controlled bloom inception and evolution: intersection of upwelling Kelvin and Rossby waves caused the dramatic thermocline shoaling and bloom inception in the central equatorial Pacific; advection by the EUC spread the bloom 4500 km east of its origin; advection by meridional currents

of short Rossby waves transported the bloom hundreds of kilometers north and south of the equator [Chavez *et al.*, 1999; Ryan *et al.*, 2002; Polito and Sato, 2003]. Since the 1998 bloom, the equatorial Pacific has been closely observed through two more El Niño events. Large-scale blooms, statistically distinguished in the ongoing record of satellite observations, occurred in 2003 and 2005, following the peaks of El Niño events in 2002 and 2004. While the thermocline and EUC were exceptionally shallow from 1998 to 2001, the large-scale blooms occurred only in the years of El Niño termination: 1998, 2003 and 2005. This pattern suggests that large-scale equatorial blooms cannot be explained only by local physical variability along the equator, i.e., variability that influences local nutrient supply to the euphotic zone. In this contribution, we present evidence that ENSO-related variability in the circulation of the western tropical Pacific may significantly alter nutrient composition of EUC source waters, thereby modulating the occurrence large-scale blooms in the central and eastern equatorial Pacific, where EUC waters enter the euphotic zone.

2. Western Pacific Modulation of Biogeochemical Dynamics in the Central and Eastern Equatorial Pacific

[5] At its origins in the western equatorial Pacific, the EUC derives most of its source waters from the New Guinea

Coastal Undercurrent (NGCUC) that transports high-salinity waters from the Solomon Sea to the EUC along the northern New Guinea margin [Lindstrom *et al.*, 1987; Tsuchiya *et al.*, 1989] (Figure 1a). Lithogenic origin of iron in the EUC is indicated by elevated concentrations of particulate iron, aluminum and manganese [Coale *et al.*, 1996a; Gordon *et al.*, 1997]. Lithogenic input of iron to EUC source waters may occur through hydrothermal venting [Gordon *et al.*, 1997], tectonic and volcanic processes [Wells *et al.*, 1999], and fluvial flux, - either directly from river outflow into the NGCUC that flows close to the New Guinea coast or indirectly as river-borne sediments deposited on the shelf and upper slope are entrained by ocean margin circulation [Milliman *et al.*, 1999; Sholkovitz *et al.*, 1999; Mackey *et al.*, 2002]. On different temporal and spatial scales, each of these potential sources may have significant variability, and hence consequences for equatorial productivity. On the timescales of ENSO, variability in ocean-atmosphere circulation and rainfall in the western tropical Pacific suggest the importance of understanding variation in fluvial transport and its intersection with the processes determining ocean margin deposition and transport.

[6] While the island of New Guinea comprises <1% of the land area draining into the global ocean, its geological and climate conditions result in an annual sediment discharge that is ~10% of the global total [Milliman *et al.*, 1999; Sholkovitz *et al.*, 1999]. About half of this discharge (860 million ton yr⁻¹) is delivered to northern coastal waters in the vicinity of the NGCUC. Extensive measurements of iron off northern New Guinea indicate that iron enters the NGCUC primarily from sediments deposited by rivers on the New Guinea shelf [Mackey *et al.*, 2002]. Key points from this study include the following: (1) Total dissolvable iron concentrations (dissolved plus labile particulate) in the NGCUC increase as it flows north along the New Guinea shelf and slope, but there are no known hydrothermal sources along the New Guinea margin that are shallow enough to contribute iron to the NGCUC. (2) Iron enrichment in the NGCUC, and the highest iron concentrations measured in the western EUC, were observed during severe drought in the western equatorial Pacific caused by El Niño. The very low river flow from New Guinea during this period suggests that riverine flux directly into the NGCUC is not the primary process supplying iron to the NGCUC. (3) Elevated concentrations of iron have been observed at 100–150 m depth (outer shelf) and up to 50 km offshore, and turbidity maxima have been observed near the shelf break 150 km from the nearest direct riverine source. Similar turbidity maxima, enriched in iron, have been observed adjacent to the continental shelf off California [Martin and Gordon, 1988]. Thus changes in the depth and strength of the NGCUC, in particular NGCUC coupling to sediments of the New Guinea shelf and upper slope, may significantly influence iron supply to the equatorial Pacific.

[7] ENSO modulation of iron supply to the equatorial Pacific, involving complex relationships between meteorologic, hydrologic, and oceanographic variability in the western tropical Pacific around New Guinea, has been considered [Sholkovitz *et al.*, 1999], and ENSO modulation of NGCUC transport has been observed [Ueki *et al.*,

2003]. Further, a relationship between El Niño and iron concentrations in the EUC is suggested by measurements of iron during two El Niño years and one La Niña year [Mackey *et al.*, 2002]. The highest iron concentrations in the EUC in the western Pacific (between 150°E and 155°E) were measured in August 1997, near the height of the 1997–1998 El Niño. The next highest iron concentrations were observed in 1993, during the end of a weaker El Niño. The lowest iron concentrations were observed in 2000, during a strong La Niña. These measurements were made at different phases of the annual cycle in NGCUC flow, thus they cannot be attributed specifically to interannual variability. The peak total dissolvable iron concentrations measured during the 1997–1998 El Niño were more than 2 nM greater than those measured during La Niña in 2000. According to model studies by Wells *et al.* [1999], a difference of this magnitude in source waters of the EUC is sufficient to fuel intense blooms along the equator. The impacts of iron introduced in the western equatorial Pacific on phytoplankton productivity in the eastern equatorial Pacific depends not only upon the amount introduced, but also upon its form and the efficiency of its transfer from west to east in the EUC. We will consider these important aspects in the discussion, after relevant physical and biological oceanographic patterns are detailed in the results.

3. Data, Methods, and Model

3.1. Niño 3.4 Sea Surface Temperature (SST) Index

[8] To describe ENSO cycles, we used the Niño 3.4 SST index, a measure of sea surface temperature anomalies in the central equatorial Pacific, over the region 120°W to 170°W, 5°N to 5°S. Monthly averages were smoothed with a 5-month running mean.

3.2. Equatorial Surface Chlorophyll Concentration

[9] To investigate variation in surface ocean phytoplankton abundance in the equatorial Pacific, we examined satellite imagery of surface chlorophyll concentrations from the Sea-viewing Wide Field-of-view Sensor (SeaWiFS) [Hooker *et al.*, 1992]. Specifically, we used version 5.1, 9-km global maps as 8-day and monthly averages. Maps are presented to illustrate mean conditions and the extremes associated with ENSO. To identify the unusual blooms, we derived a time series of average chlorophyll between 2°N and 2°S, computed means and standard deviations (SD) at each longitude, and identified exceptionally high values as more than 2 SD above the mean. Because chlorophyll concentrations are approximately lognormally distributed, these computations were done with log-transformed chlorophyll values.

3.3. Equatorial Winds, Ocean Currents, and Temperatures

[10] To examine variation in equatorial winds, ocean currents and temperature relative to development of the blooms, we used observations from the equatorial moorings of the Tropical Atmosphere Ocean (TAO) array [McPhaden *et al.*, 1998] and satellite SST data. Time series of monthly average zonal wind velocity defined the strength of local

wind-driven upwelling. Monthly average zonal ocean current velocity data from Acoustic Doppler Current Profilers (ADCP) on the equator within the bloom domains (140°W and 110°W) defined variation in the strength and shoaling of the EUC. To represent the mean profile of the Equatorial Undercurrent, we averaged monthly mean ADCP profiles of zonal velocity at 165°E, 140°W and 110°W on the equator, for the full duration of the ADCP records. Observations began in 1990 at 140°W, and in 1991 at 165°E and 110°W. All available observations up to late 2005 were averaged to produce the mean profiles, which were smoothed with a three-point (15 m) running mean (Figure 1b). TAO temperature and velocity measurements on the equator were used to illustrate the water column temperature distribution and EUC core depth underlying each bloom. To examine SST variation along the equator relative to variation in surface chlorophyll concentrations, we used Reynolds and Smith Version 2 (RSV2) optimally interpolated weekly SST data for 1997 through 2005, averaged between 2°N and 2°S. To represent mean SST in the tropical Pacific (Figure 1a), we averaged monthly RSV2 SST maps for 1971 to 2000.

3.4. Equatorial Thermocline Depth

[11] To illustrate thermocline (nutricline) depth variation, we used TAO dynamic height and sea surface height anomaly (SSHA) data from the TOPEX/Poseidon [Fu *et al.*, 1994] and Jason-1 satellite altimeters. Because the upper ocean temperature profile is the dominant control of the density profile in the equatorial Pacific [Polito *et al.*, 2000], thermocline depth variation is evident in dynamic height and SSHA. Analysis of a 9-year time series at 10-day resolution showed that TOPEX SSHA explained between 73% and 93% of the variance in the depth of the 20°C isotherm (center of the thermocline) measured at TAO moorings along the equator [Ryan *et al.*, 2002]. At all mooring locations east of 170°W, where blooms occurred in all three years, SSHA explained more than 80% of the variance in the depth of the 20°C isotherm. SSHA is therefore a good basis for describing thermocline depth variation relative to the blooms, and it has the advantages of greater spatial coverage and more consistent temporal coverage than the TAO moorings (the moorings are widely spaced and their time series have gaps). To generate a consistent time series for 1997 through 2005, we acquired the 6-km along-track gridded SSHA at 10-day resolution and bin-averaged SSHA between 2°N and 2°S at a zonal resolution of 5° longitude. Because the Jason-1 altimeter replaced TOPEX on its orbital path, TOPEX data were used until its orbit changed in August 2002, and Jason-1 data were used thereafter.

3.5. New Guinea Coastal Undercurrent (NGCUC)

[12] To examine variation in the NGCUC, we used moored and shipboard ADCP measurements of ocean current velocity made between July 1995 and January 2005. Shipboard measurements across the NGCUC, along 142°E, were conducted during cruises, usually twice a year during boreal summer and winter. A mooring at 2.5°S 142°E, ~50 km north of the New Guinea coast, 40 km north of the shelf break, and in the NGCUC path, was equipped with an upward looking RD Instruments 150-kHz ADCP. The ADCP current velocity data were at

hourly resolution between 30 and 300 m depth, and they were corrected by conductivity-temperature-depth time series measurements [Ueki *et al.*, 2003]. Between July 1995 and January 2005, there was a single gap in measurements during August 2000 to December 2001.

3.6. West to East Transport Rate Estimation and Validation

[13] To determine if the observed temporal lag between NGCUC shoaling/intensification and the equatorial blooms could be explained by transport of iron in the NGCUC/EUC, we estimated transport rates and compared them with measured velocity profiles. The initial transport rate estimate was based on distance and time: distance along the equator from the NGCUC/EUC confluence to a fixed reference point at 110°W (where all blooms were strongly pronounced), and estimated time between arrival of potentially iron-enriched waters at the confluence and bloom inception. To validate these transport rate estimates, we analyzed moored ADCP current velocity measurements off New Guinea and along the equator.

[14] The first computation was to estimate transport rates from New Guinea to the equator. For this we used distance along the approximated NGCUC path and average velocity profiles of the shoaled/enhanced NGCUC measured by the moored ADCP. Temporally averaged profiles were computed from hourly velocity measurements and centered on the alongshore-equatorward current maximum (i.e., the core of the NGCUC). From the average profiles, average velocity was computed over the 100-m thick layer centered on the NGCUC core. This scale was chosen because it is the approximate vertical scale of iron enrichment evident in the NGCUC and EUC (based on profiles published by Gordon *et al.* [1997] and Mackey *et al.* [2002]). For the 1997–1998, 2002–2003 and 2004–2005 El Niño events, these velocities were 70, 64 and 62 cm s⁻¹, respectively. A time range for arrival of potentially iron-enriched NGCUC waters at the 2.5°S mooring was defined as (1) early, 1 month after the initial shoaling and enhancement of the NGCUC (allowing time for current-shelf interactions along the New Guinea margin to result in iron-enriched waters), and (2) late, the maximum of the NGCUC enhancement (defined from the low-pass filtered time series). Time for these waters to reach the equator from 2.5°S was then estimated from the NGCUC path distance north of 2.5°S and ADCP-based transport rates.

[15] The second computation was to estimate transport rates along the equator from the NGCUC confluence to 110°W. For the first two blooms, four equatorial moorings between New Guinea and 110°W (165°E, 170°W, 140°W, and 110°W) had full ADCP records for the periods between NGCUC enhancement and the bloom starts. For each of these moorings, (1) each daily eastward current maximum in the thermocline was defined as the center of the EUC, (2) temporally averaged profiles were computed over the 100-m-thick layer centered on the EUC core, and (3) the temporal and depth-averaged speed was computed from the temporally averaged profiles. The average result of step 3 from the four moorings was then compared with the independent rate estimates based on timing of NGCUC shoaling/intensification and the blooms.

3.7. Three-Dimensional Ocean Circulation Model Simulations

[16] Using the Regional Ocean Modeling System (ROMS), we developed a Pacific Ocean configuration with 12.5-km horizontal resolution and 30 vertical layers. ROMS [Shchepetkin and McWilliams, 2005] solves the primitive equations in an Earth-centered rotated Cartesian coordinate system. The Boussinesq approximation (i.e., where density variations are neglected everywhere except in the gravitational force) is used. ROMS is discretized on coastline- and terrain-following curvilinear coordinates. ROMS is a split-explicit, free-surface ocean model, where short time steps are used to advance the surface elevation and barotropic momentum, with a much larger time step used for temperature, salinity, and baroclinic momentum. A nonlocal, K profile parameterization (KPP) is used for vertical mixing [Large *et al.*, 1994]. ROMS was written as a parallel code, which uses 2-D partitioning of the model grid into subdomains that may be assigned to different processors. The distributed memory (MPI) ROMS version is used in this study using 128 computing processors.

[17] Starting from the climatological temperature and salinity conditions at rest, the Pacific ROMS was integrated for thirty years forced with the monthly climatological air-sea fluxes. After this 30-year spin-up, the Pacific ROMS was integrated during 1992–2004, forced with the daily air-sea fluxes derived from NCEP reanalysis [Kalnay *et al.*, 1996]. The 3-day mean model output was saved for the analysis presented in this study.

4. Results

[18] In this section we will first examine SeaWiFS satellite-based chlorophyll estimates (Chl) to illustrate the strong biological variation associated with ENSO, to define how the blooms following three successive El Niño events are unique in the record, and to characterize differences in the scales and locations of the blooms. We will then use observations of equatorial physical conditions and circulation to show that the occurrence of large-scale blooms following the three most recent El Niño events cannot be explained simply by anomalous local physical forcing (thermocline/EUC depth or winds). Examining observed circulation of the NGCUC between 1995 and 2005, we will show consistent ENSO-modulated intensification of NGCUC flow. Last, using results from a high-resolution 3-D ocean circulation model we will illustrate meander and eddy formation at the shelf break associated with NGCUC intensification, augmenting coupling of the New Guinea margin to the EUC, and we will validate the model eddy description using satellite altimeter observations. Together, the observational and model results describe a plausible mechanism of biogeochemical forcing underlying the equatorial blooms closely following El Niño.

[19] Elevated levels of phytoplankton biomass across the region influenced by equatorial upwelling are evident in climatological Chl (Figure 2a). Depressed Chl over much of this region occurred during the three most recent El Niño events, and large-scale blooms followed each of these events (Figures 2b–2d). The Niño 3.4 index, sea surface temperature (SST) anomalies in the central and eastern equatorial Pacific, identifies peaks of recent El Niño events

late in 1997, 2002 and 2004 (Figure 2e). Chl in the eastern equatorial Pacific was exceptionally high in 1998, 2003 and 2005 (Figure 2e). The magnitude of the blooms corresponded with the strength of the El Niño events that preceded them. The strongest El Niño and bloom occurred in 1997–1998, the next strongest in 2002–2003, and the weakest in 2004–2005.

[20] Where the large-scale blooms occurred along the equator was closely related to where the EUC and thermocline shoaled in the east (Figure 3). During the 1998 and 2003 blooms (Figures 3a and 3b), the maximum surface chlorophyll concentrations coincided with the shallowest EUC depths (triangles). During the 1998 bloom, thermocline waters (shaded) outcropped to the surface ~3000 km further west than during the 2003 and 2005 blooms, and the EUC was ~40–50 m shallower at 140°W during the 1998 bloom than during the 2003 and 2005 blooms. These strong thermocline and EUC depth anomalies in 1998, coincident with inception of the bloom across ~2500 km, were forced by intersection of upwelling Kelvin and Rossby waves [Ryan *et al.*, 2002]. Acting atop the basin-scale west-to-east shoaling of the thermocline and EUC (Figure 1b), vertical displacement of the thermocline by Kelvin and Rossby waves strongly influence the spatial and temporal distribution of nutrient supply to the euphotic zone. We will consider whether exceptional thermocline shoaling is the single consistent factor underlying all of the large-scale blooms.

[21] Local thermocline depth variation can be examined with a time series of dynamic height from the TAO mooring at 110°W, where all blooms were pronounced (Figure 4). Shallow thermocline (nutricline) anomalies are indicated by low dynamic height. A gap in the 110°W mooring record precludes direct comparison of dynamic height and surface chlorophyll during the 1998 bloom. However, the available record suggests that the lowest dynamic height anomalies occurred at the end of 1998, months after the local bloom peak. This interpretation is consistent with the development of the coldest Niño 3.4 SST anomalies at the end of 1998 (Figure 2e). In previous studies, the local bloom peak east of 140°W in 1998 was related to eastward advection of the bloom environment in the EUC, not eastward spread of shallow thermocline anomalies [Chavez *et al.*, 1999; Ryan *et al.*, 2002]. In contrast, the blooms at 110°W during 2003 and 2005 coincided with local thermocline shoaling. During 2003 (Figure 4b), two rapid increases in chlorophyll concentrations beginning in April and May occurred during the periods of most rapid decreases in dynamic height (most rapid thermocline shoaling). Similarly, during July–August 2005 (Figure 4c), the rapid increase in chlorophyll occurred during a period of rapidly decreasing dynamic height. Therefore the 2003 and 2005 blooms are consistent with local thermocline influence on bloom development.

[22] Although the record at 110°W (Figure 4) supports the importance of local thermocline depth variation on development of the blooms, it also introduces a puzzle. If local thermocline shoaling was the sole cause of blooms, we would expect blooms to have occurred during late 1998 and the second half of 1999, when local dynamic height was much lower than during the 2003 and 2005 blooms (Figure 4a). Consideration of this puzzle requires detailed examination of biological and physical variation along the

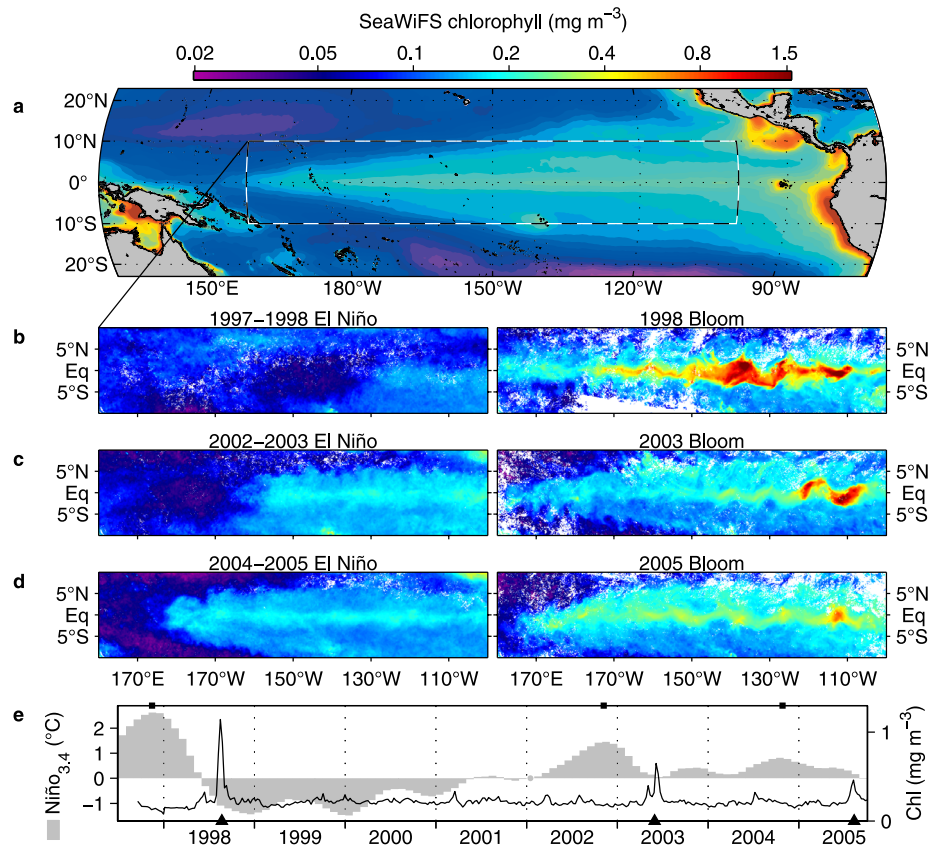


Figure 2. Variation in surface chlorophyll concentrations (Chl) from the Sea-viewing Wide Field-of-view Sensor (SeaWiFS) satellite instrument. (a) Climatological Chl for November 1997 through October 2005. (b) Low Chl during the 1997–1998 El Niño (December 1997) and the bloom that followed (5–12 August 1998). (c) Low Chl during the 2002–2003 El Niño (November 2002) and the bloom that followed (2–9 June 2003). (d) Low Chl during the 2004–2005 El Niño (December 2004) and the bloom that followed (5–12 August 2005). (e) Niño 3.4 sea surface temperature anomalies in the tropical Pacific (shaded); black squares along the top time axis indicate peaks of recent El Niño events. Chl (line) is 8-day average SeaWiFS chlorophyll between 2°N and 2°S, 110°W to 115°W. Black triangles along the bottom time axis indicate the local bloom peaks.

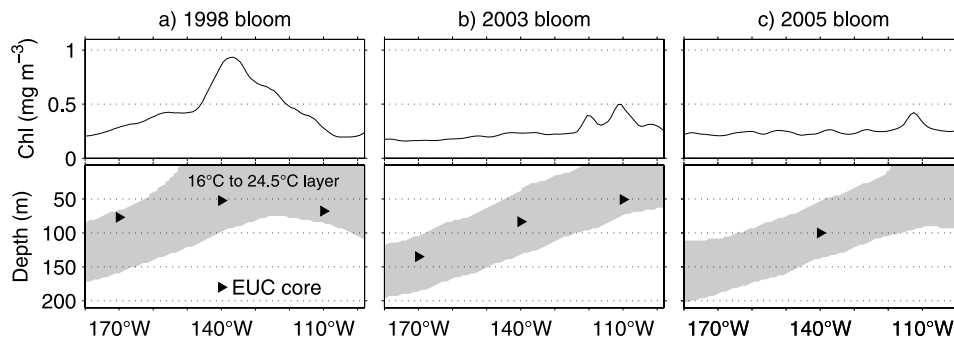


Figure 3. Location of bloom maxima relative to where thermocline/EUC waters shoaled in the central and eastern equatorial Pacific. (a, top) 2°N to 2°S average SeaWiFS chlorophyll (Chl) during the 1998 bloom peak. (bottom) Water temperatures between 16°C and 24.5°C (shaded) and the depth of the EUC core (triangles) underlying the bloom peak. (b) As in Figure 3a during the 2003 bloom peak. (c) As in Figure 3a during the 2005 bloom peak. Sufficient velocity observations are not available to characterize the EUC core at all three longitudes during 2005.

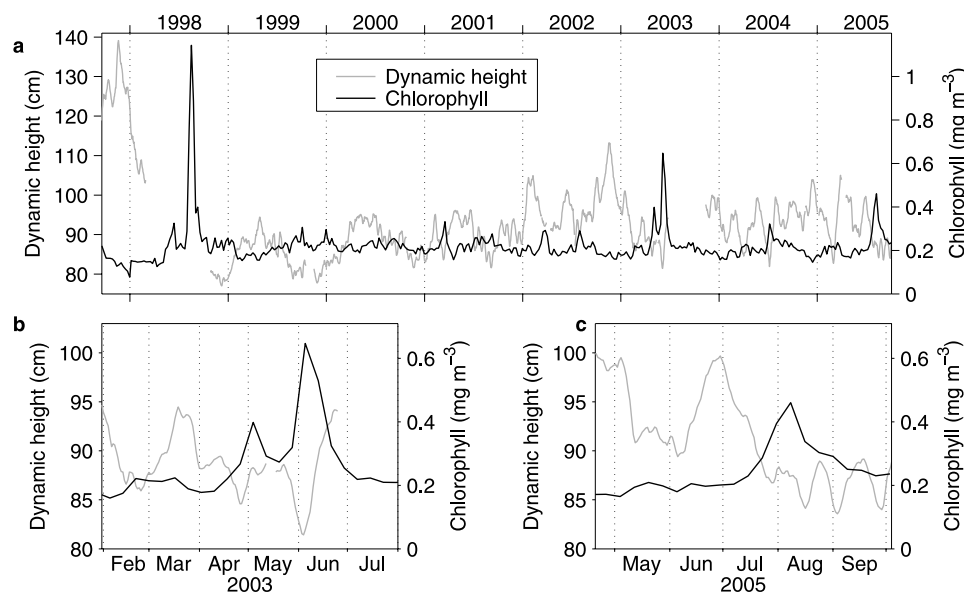


Figure 4. Variation in dynamic height and SeaWiFS chlorophyll at 110°W on the equator. Dynamic height was computed from TAO temperature profiles by vertically integrating the specific volume anomaly from the surface to 500 m depth (results provided by the TAO Project). Low dynamic height indicates shallow thermocline depth. Chlorophyll concentrations are as in Figure 2e. (a) Full record and (b, c) details of the 2003 and 2005 blooms.

equator at high spatial and temporal resolution (Figure 5). Exceptional blooms, defined as Chl more than 2 standard deviations above the mean (based on log-transformed Chl, which is approximately normally distributed), occurred only during 1998, 2003 and 2005 (Figure 5a). This time series also shows the low Chl anomalies of the El Niño events and their differing spatial scales and magnitudes, consistent with the differing spatial scales and magnitudes of the blooms that followed El Niño. The space-time domains of the blooms from Figure 5a are overlaid on sea surface height anomalies (SSHA) in Figure 5b; shallow thermocline anomalies are evident as low SSHA. The lowest SSHA occurred during 1998–2001 in the central and eastern equatorial Pacific; these were much lower than SSHA that coincided with the 2003 and 2005 blooms. Consistent with the SSHA variation, colder equatorial SST prevailed during 1999–2001 than during the 2003 and 2005 blooms (Figures 5c and 2e). Also, eastward flow of the EUC was stronger and shallower during 1999 through 2001 than during the 2003 and 2005 blooms (Figure 6). Last, the easterly winds (negative zonal winds in Figure 5d) that drive equatorial upwelling were not unusually strong during any of the bloom periods, considering interannual or seasonal timescales. In summary, no observations of the physical environment along the equator support the conclusion that local physical variability can explain the consistent occurrence of large-scale blooms following El Niño events.

[23] Consistent occurrence of these blooms following El Niño may be explained by changes in circulation of the NGCUC during El Niño (Figure 7). After flowing northward along the northern New Guinea margin, the NGCUC contributes most of the source waters to the EUC at its origins in the western equatorial Pacific [Lindstrom *et al.*, 1987; Tsuchiya *et al.*, 1989]. Measurements of NGCUC flow from moorings and ships show strong seasonal vari-

ation caused by monsoonal winds [Ueki *et al.*, 2003]. Flow is strongest during summer, and average summer conditions (Figure 7b) show alongshore/equatorward NGCUC flow maximal between ~ 170 and 300 m depth. The mean flow derived from our observations is consistent with previous studies showing the NGCUC core at and below 200 m depth with core speeds of $50\text{--}60\text{ cm s}^{-1}$ [Lindstrom *et al.*, 1987; Tsuchiya *et al.*, 1989; Kuroda, 2000; Cresswell, 2000; Johnson *et al.*, 2002]. During both the 1997–1998 (Figure 7c) and 2002–2003 (Figure 7d) El Niño events, the NGCUC exhibited three changes of significance to iron transport from the New Guinea shelf: (1) core current velocity increased to $\sim 100\text{ cm s}^{-1}$, well above the normal annual maximum of $60\text{--}70\text{ cm s}^{-1}$, (2) the core of the current shoaled to the depth of the outer shelf (centered between 100–150 m depth), and (3) the current broadened. Mackey *et al.* [2002] presented velocity sections across the NGCUC during the 1997–1998 El Niño (August 1997) along four longitudes between 143°E and 145°E . These sections all show a strong, shallow NGCUC similar to our section along 142°E (Figure 7c). Although no comparable ship section was surveyed in 2005, moored current velocity measurements in the NGCUC show that variation in its flow over the depth range of the outer shelf was closely coupled with ENSO through the period of the most recent three El Niño events. Sustained intensification of NGCUC flow at these depths occurred during the 1997–1998 [Ueki *et al.*, 2003] and 2002–2003 and 2004–2005 El Niño events (Figure 7e). This variation in the NGCUC closely tracked equatorial SSHA anomalies in the western Pacific north of New Guinea, and equatorial SST anomalies in the central Pacific (Figure 7e).

[24] These observed changes in NGCUC flow suggest enhanced potential for entrainment of iron-bearing sediments from depositional zones on the shelf and upper slope.

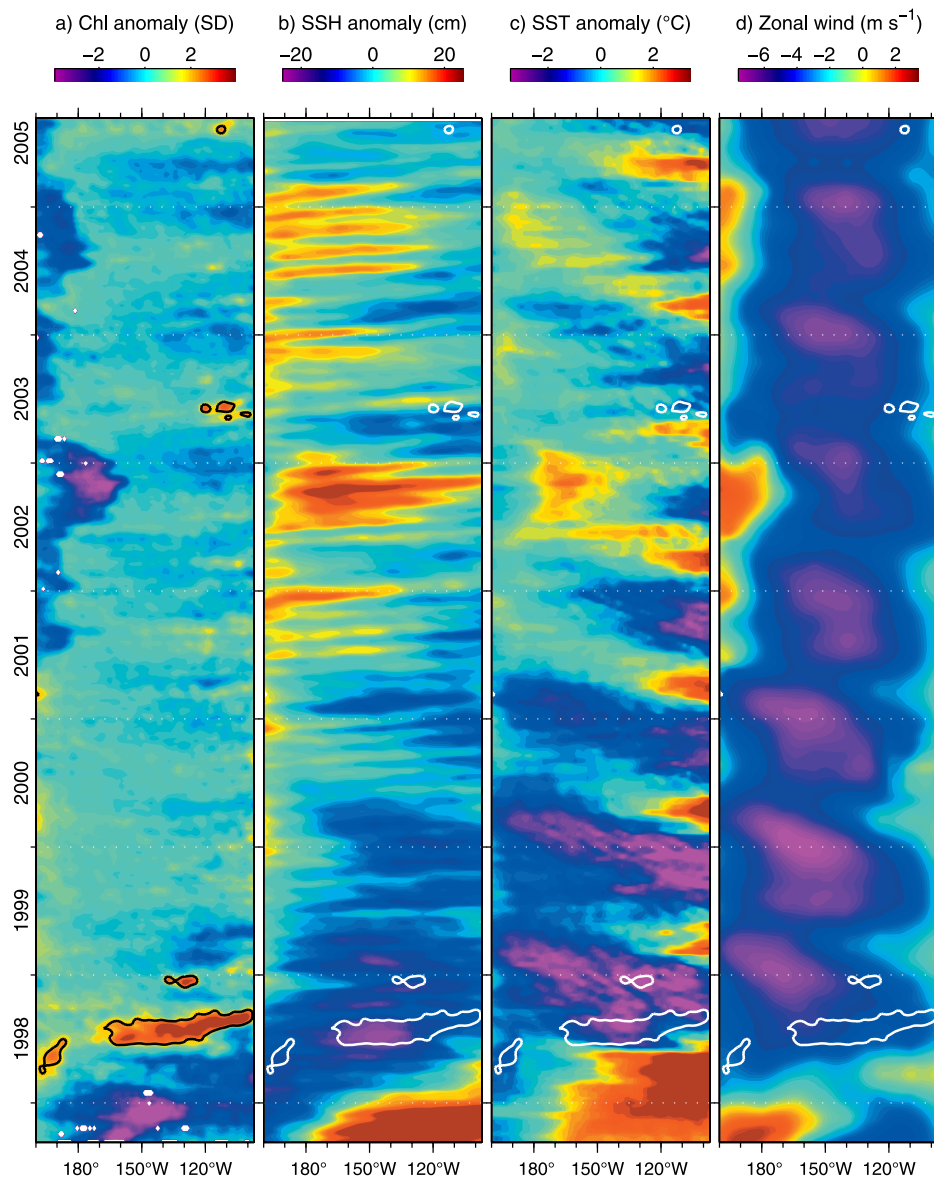


Figure 5. Spatiotemporal distribution of the blooms relative to indicators of potential local causative factors. All time series include the annual cycle as well as interannual variation. (a) Chlorophyll anomalies between 2°N and 2°S , computed as standard deviations (SD) from the long-term mean of log-transformed Chl. Blooms are defined as more than 2 SD above the mean. These bloom domains are overlaid as white contours on physical time series in Figures 5b–5d. (b) Sea surface height (SSH) anomalies between 2°N and 2°S from satellite altimetry. Negative SSHA indicate shallow thermocline anomalies; positive SSHA indicate deep thermocline anomalies. (c) Sea surface temperature (SST) anomalies between 2°N and 2°S , computed as deviations from the long-term mean of optimally interpolated satellite-derived SST data. (d) Zonal winds averaged between 2°N and 2°S ; negative zonal winds are upwelling favorable.

While the 10-year time series of NGCUC observations defines a phenomenon of interest for considering western Pacific modulation of iron flux and equatorial blooms, the observational resources are not sufficient to examine the nature of changes in NGCUC-shelf coupling. However, high-resolution ocean circulation modeling affords this opportunity. The model accurately simulated mean flow of

the NGCUC (Figure 8a), as well as interannual variation in current flow near the shelf break during the growing phase of the 2003–2003 El Niño (Figure 8b). Zonal velocity at 150 m from days 135 and 225 (times indicated in Figure 8b) illustrate shoaling and intensification of the NGCUC (Figure 9a). This included the region offshore of the Sepik River, the largest river contributing sediments to the north-

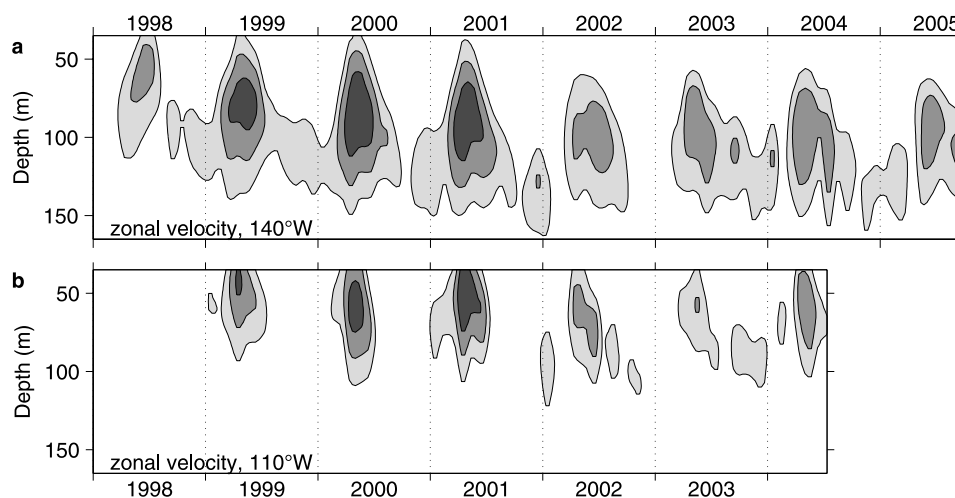


Figure 6. Variability in the depth and strength of the Equatorial Undercurrent (EUC). Contours are zonal velocity on the equator measured by acoustic Doppler current profilers (ADCP) at (a) 140°W and (b) 110°W. Shaded regions exceed 100 cm s^{-1} ; contour interval is 25 cm s^{-1} . Maximum positive values define the core of the eastward flowing EUC.

ern New Guinea shelf [Sholkovitz *et al.*, 1999; Kineke *et al.*, 2000].

[25] When the NGCUC intensified and shoaled, it developed growing meanders that formed eddies along the shelf break. Meander and eddy generation and evolution are illustrated with a time series of model salinity at 150 m (Figure 9b). Water mass distributions and circulation of one eddy are detailed (Figure 10). Meander generation consistently began between 5°S and 3°S, where coastline orientation changes (Figure 9b), and where the Sepik River deposits sediments on the shelf and upper slope. Cross-shelf exchange, indicated in the salinity distribution (Figure 10), was pronounced near the Sepik River mouth. Meander/eddy exchange occurred against the background of strong northward flow in the NGCUC, as illustrated by the current vectors (Figure 10). As they approached the eastward flowing EUC, the meanders and eddies were stretched into filaments and entrained by the EUC (Figure 9b). This modeled relationship between NGCUC intensification and shoaling, intensified meandering and eddy formation, and enhanced coupling between the New Guinea outer shelf and the EUC was evident in other periods of NGCUC intensification in the model simulation. Thus the model results indicate that the NGCUC intensification and shoaling observed during El Niño events would increase coupling of the EUC to iron sources in shelf sediments of northern New Guinea. Further, because the thermocline north of New Guinea is relatively shallow during El Niño (Figure 7e), capture of shelf sediments by the EUC may also be enhanced during these periods.

[26] The model description of cyclonic eddies off the shelf break is substantiated by synoptic maps of SSHA. For example, a cold core cyclonic eddy from late 2002, when observations and the model simulation show enhanced NGCUC flow, is shown in Figure 11. The low SSHA core of the eddy is centered at $\sim 145.3^\circ\text{E}$, 3.3°S . Within 12 hours, this eddy was sampled along intersecting altimeter tracks, and its immediately adjacent waters west and east were sampled. Therefore its structure was described synop-

tically, which is a requirement if the eddy was translating northwestward as predicted by the model.

[27] If the basis for these large-scale equatorial blooms was El Niño modulation of NGCUC flow and associated enhancement of iron concentrations in the NGCUC/EUC, then the observed time lags between NGCUC flow changes and the blooms should be consistent with measured velocity profiles of the NGCUC and EUC (Table 1). Transport speeds along the equator from the NGCUC/EUC confluence to the 110°W bloom reference point were estimated between 40 and 68 cm s^{-1} , based on transport distance and timing of NGCUC intensification and the blooms. During the period between NGCUC intensification and the blooms, measured average zonal current velocity over a 100-m-thick layer centered on the core of the EUC ranged between 55 and 59 cm s^{-1} . The vertical scale of averaging is based on the vertical scale of peak iron concentrations observed in the western EUC [Mackey *et al.*, 2002] and eastern EUC [Gordon *et al.*, 1997]. The single velocity for each event represents an average from four moorings between 165°E and 110°W, i.e., a representative average over the large zonal span across which iron-enriched waters would have been transported in the EUC. Therefore we conclude that the timing of the equatorial blooms relative to prior NGCUC intensification is consistent with observed EUC transport rates. By extension, we conclude that transport of iron-enriched waters from New Guinea shelf to the euphotic zone of the equator can occur on the observed timescales and is therefore a plausible hypothesis for explaining large-scale blooms following NGCUC intensification during El Niño events.

5. Discussion

[28] If local variability was the sole basis for large-scale blooms in the equatorial Pacific, then blooms should have occurred during 1998–2001, when the thermocline was most shallow, the EUC was most shallow and intense, and SST was coldest. Instead, large blooms occurred only after peaks of three consecutive El Niño events during which the

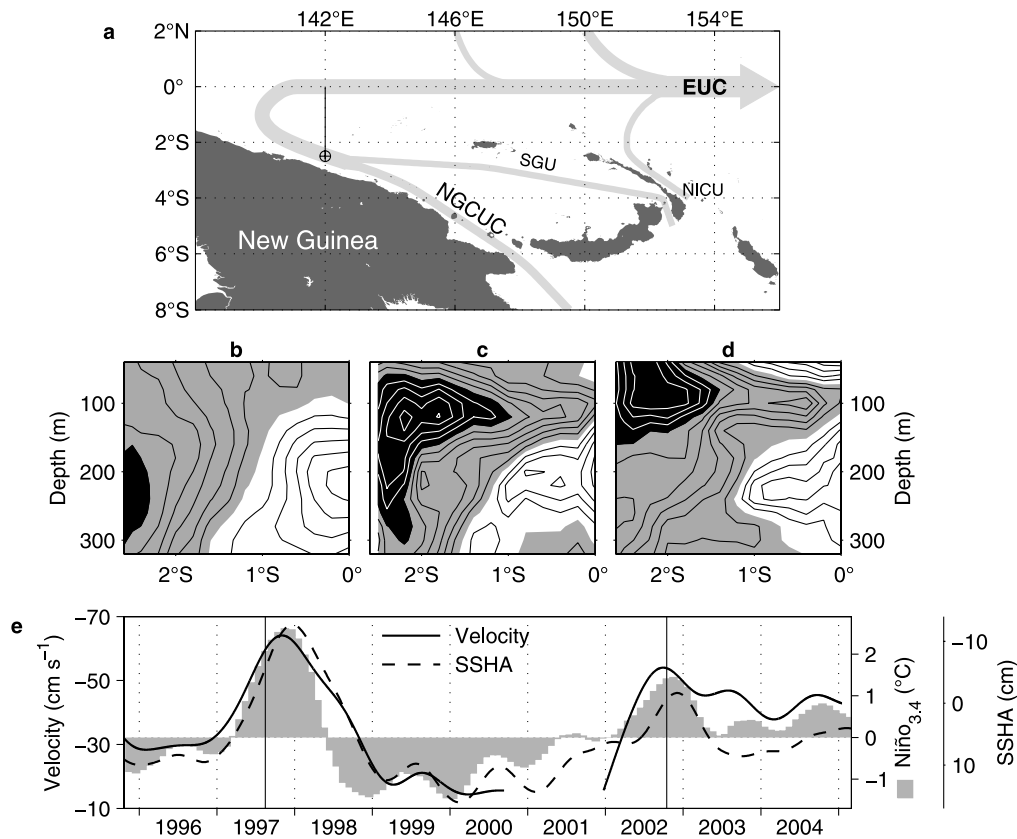


Figure 7. Variability in the New Guinea Coastal Undercurrent (NGCUC) linked to ENSO. (a) Summary of southwestern equatorial Pacific undercurrents that feed into the EUC, including the NGCUC, modified from Wells *et al.* [1999] and Sholkovitz *et al.* [1999]. Other currents are the Saint Georges Undercurrent (SGU) and New Ireland Coastal Undercurrent (NICU). The circle at 2.5°S, 142°E shows the location of a mooring that has made ADCP measurements of the NGCUC since 1995. The line between the equator and 2.5°S along 142°E shows the ship transect that has been regularly occupied for water property and current velocity measurements since 1995. (b) Vertical section of average alongshore velocity during summer from the ship transect observations. Westward alongshore flows are shaded; contour interval is 10 cm s⁻¹; the NGCUC core is shown in black. The average was computed from surveys in July 1995, July 1996, September 1998, and September 2000, which individually showed the NGCUC core centered between 200 and 250 m depth. (c) Vertical section of alongshore velocity during the 1997–1998 El Niño (August 1997). (d) Vertical section of alongshore velocity during the 2002–2003 El Niño (October 2002). (e) Alongshore equatorward velocity at outer shelf depths (50–150 m) from the mooring at 142°E, 2.5°S relative to sea surface height anomalies (SSHA) along the equator (2°N to 2°S) north of New Guinea (140°E to 150°E) and SST anomalies in the central and eastern equatorial Pacific (Niño 3.4 index). The velocity and SSHA time series were low-pass filtered with a cutoff of 380 days to emphasize interannual variation. Vertical lines mark the times of ship-based velocity sections shown in Figures 7c and 7d.

thermocline in the western equatorial Pacific was anomalously shallow, and the New Guinea Coastal Undercurrent was anomalously shallow and intense. The primary pattern of the eastern equatorial Pacific coincident with all three blooms was with the location of thermocline and EUC venting to the euphotic zone. As nutrient-rich waters are transported eastward across the equatorial Pacific, they approach the euphotic zone because of the basin-scale slope of the thermocline and EUC. Numerous physical processes can act upon this basin-scale shoaling of nutrient source waters to influence local rates of vertical nutrient transport [Ryan *et al.*, 2002]. Inception of the 1998 bloom coincided

with very shallow thermocline depth forced by intersection of upwelling Rossby and Kelvin waves [Ryan *et al.*, 2002], and initiation of the 2003 and 2005 blooms coincided with rapid local thermocline shoaling events. This physical-biological coincidence indicates the importance of local nutrient flux in determining when and where the bloom began, but it cannot explain the observed limitation of large blooms to three periods in the 8-year record: only following the termination of three consecutive El Niño events.

[29] Together, the time series observations and model simulations provide a plausible hypothesis for modulation of large-scale blooms in the equatorial Pacific on the

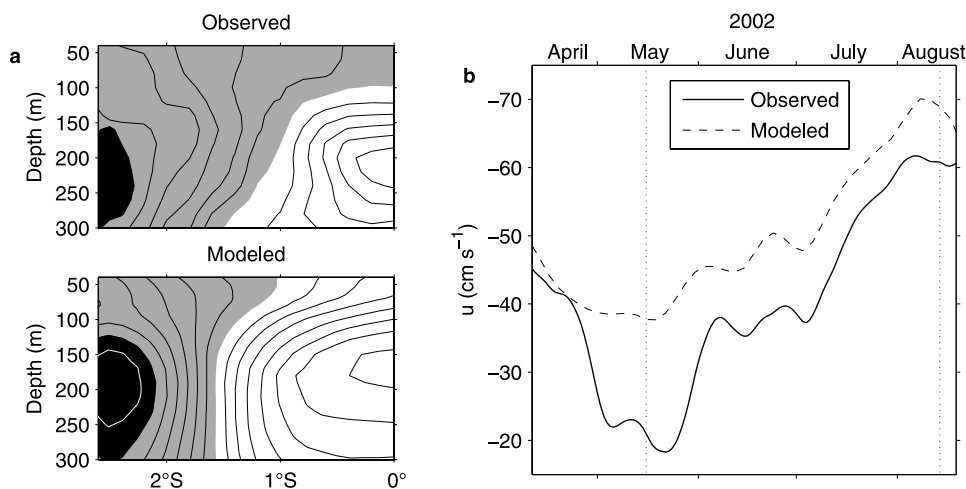


Figure 8. Comparison of observed and modeled NGCUC flow. (a) Observed and modeled zonal velocity during summer. Observed mean flow was computed from surveys in July 1995, July 1996, September 1998, and September 2000. Modeled mean flow was computed from simulation results during June–September from model years 2001 and 2003 (excluding the anomalous El Niño summer of 2002). Shading and contours are as in Figure 7b. (b) Observed and modeled average zonal current speed in the layer 50 to 150 m. Both time series were low-pass filtered with a 33-day cutoff. Higher negative values indicate stronger NGCUC flow. The vertical dotted lines mark the times for which maps of zonal velocity at 150 m depth are presented (Figure 9a).

timescale of ENSO. Shoaling and intensification of the NGCUC occurred consistently during the last three El Niño events, in coincidence with the strongest sea surface height and temperature anomalies in the eastern and western equatorial Pacific. Shelf sediments of northern New Guinea are considered to be the primary iron source for the NGCUC/EUC [Mackey *et al.*, 2002]. NGCUC shoaling

and intensification alone may enhance transport of iron from shelf sediments into the EUC by increasing direct contact of the NGCUC with outer shelf sediment deposition zones. However, our model simulations indicate that meanders and eddies of the intensified NGCUC augment cross-shelf fluxes at the depth of the outer shelf and upper slope in regions known to host fluvial sediment deposition, and these

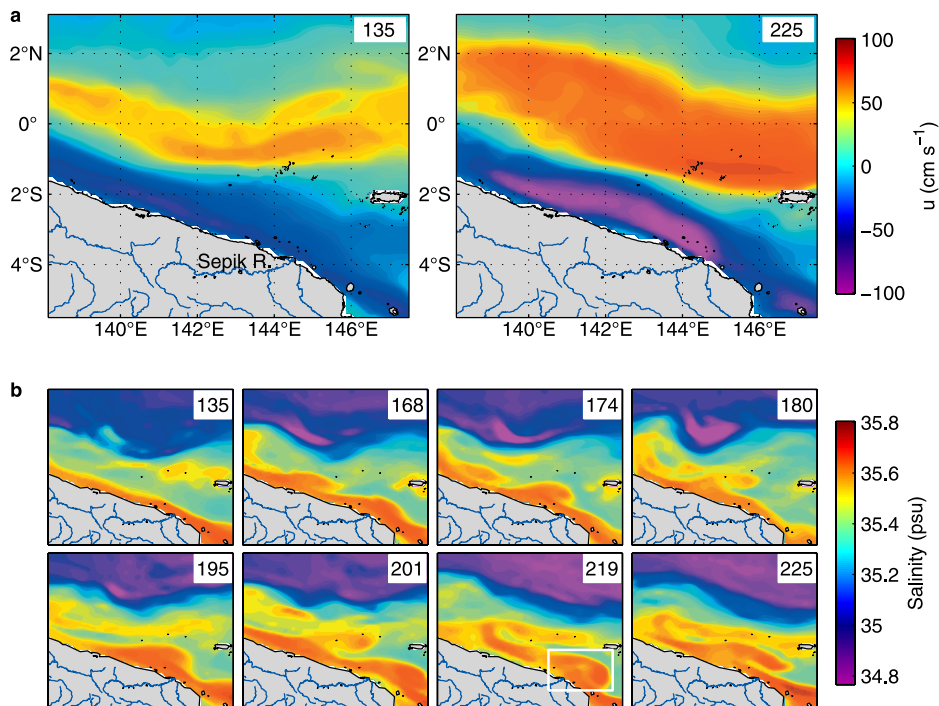


Figure 9. Modeled behavior of the NGCUC during the period of current intensification shown in Figure 8b. (a) Maps of zonal velocity at 150 m depth on days 135 and 225 of 2002 (times indicated in Figure 8b). (b) Maps of salinity at 150 m depth between days 135 and 225. The day is labeled in each panel.

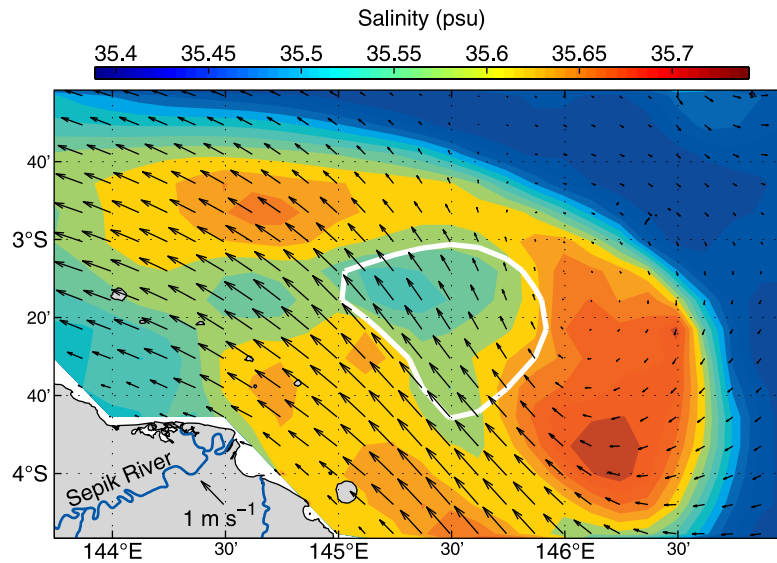


Figure 10. Indication of cross-shelf exchange associated with a modeled NGCUC cyclonic eddy (box in Figure 9b, day 219). Variables represented at 150 m depth are salinity (color map), velocity (vectors), and the cold core of the eddy (waters within the white contour are $<18.25^{\circ}\text{C}$).

dynamics appeared to enhance direct coupling of the New Guinea shelf and upper slope to the EUC. The observed lag between NGCUC intensification and the equatorial blooms can be explained by the observed flow of the NGCUC and EUC. In this hypothesis, the large-scale blooms result from local variability at the equator acting upon an Equatorial Undercurrent that experiences interannual variation in nutrient composition.

[30] The impacts of iron introduced in the western equatorial Pacific on phytoplankton productivity in the eastern equatorial Pacific depends upon the amount of iron introduced, the efficiency of its transfer to the eastern equatorial Pacific euphotic zone, and its bioavailability. The observed and modeled processes should result in substantial increases in sediment transport, particularly if NGCUC eddies are consistently generated where the coastline orientation changes near the mouth of the largest river on the northern coast, the Sepik River. Sediment deposition zones reside in a submarine canyon that meets the Sepik River mouth and on the outer shelf and upper slope west of the river mouth [Kineke *et al.*, 2000]. Efficiency of iron transfer into the EUC may be augmented by shoaling of the equatorial thermocline north of New Guinea that coincides with the intensified NGCUC dynamics. Phytoplankton readily use dissolved iron, and some dissolved iron may accompany sediment transport. However, the majority of iron entrained by the NGCUC is thought to be in particles and colloids that are included in the measurement of total dissolvable iron [Sholkovitz *et al.*, 1999; Mackey *et al.*, 2002]. Iron in this form is not readily used by phytoplankton, but it can become bioavailable through photoreduction [Johnson *et al.*, 1994], phagotrophy [Barbeau and Moffett, 2000], dissociation [Kuma *et al.*, 2000], and reduction at phytoplankton cell surfaces (literature summarized by Sunda [2001]). Therefore much of the iron supplied by New Guinea shelf sediments may be considered as ultimately bioavailable [Mackey *et al.*, 2002]. In coastal waters of the California Current upwelling system, transport of shelf

sediments into the euphotic zone is a primary iron source [Johnson *et al.*, 1999], and the observation of large decreases in the Fe/Al ratio of particles from coastal upwelling provides evidence that some of the particulate iron is consumed [Johnson *et al.*, 1997].

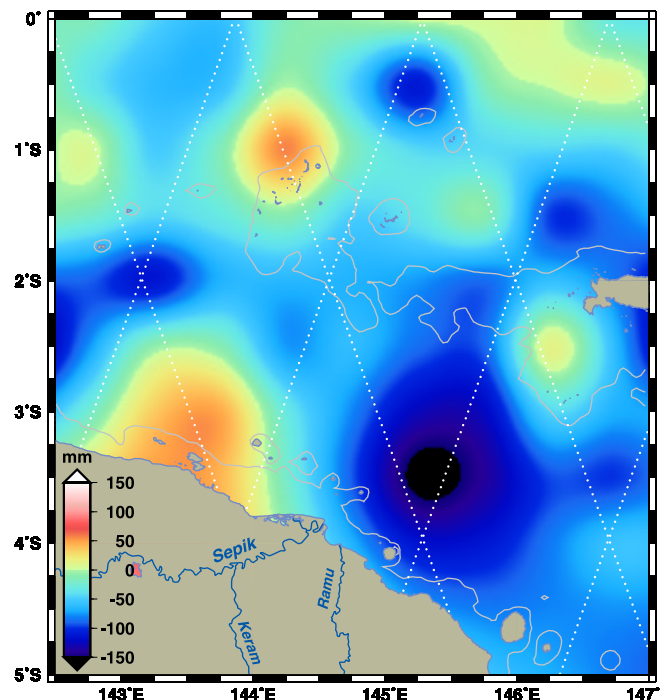


Figure 11. Observation of a cyclonic eddy along the northern New Guinea margin during the 2002–2003 El Niño. The map shows the SSHA off northern New Guinea from the TOPEX and Jason satellite altimeters for the 10-day period centered on 24 October 2002; gridded using GMT [Smith and Wessel, 1990]. The white dots show the locations of the 6-km along-track grid points of SSHA. The contour north of New Guinea is the 1000 m isobath.

Table 1. Estimated Rates of EUC Transport From New Guinea to the 110°W, 0°N Reference Point, Where All Equatorial Blooms Were Pronounced^a

El Niño Event	NGCUC Shoaling and Peak Intensification	Equatorial Bloom Start at 110°W	Estimated Transport Rate, cm s ⁻¹	Measured EUC Velocity, cm s ⁻¹
1997–1998	17 July 1997, 4 November 1997	7 August 1998	40–53	55
2002–2003	5 July 2002, 29 September 2002	3 May 2003	53–68	59
2004–2005	18 July 2004, 24 September 2004	28 July 2005	42–47	-

^aThe date of NGCUC shoaling is based on moored current measurements from 2.5°S, 142°E (Figure 7a). The date of NGCUC peak intensification is based on low-pass filtered average velocity between 50 and 150 m depth (Figure 7e), which defines the center of the period of NGCUC shoaling and enhanced flow. The bloom start dates are the times at which exceptionally high chlorophyll concentrations were first observed at the reference point of 110°W (Figure 2e). Transport velocity was estimated from distance and time: distance along the equator between the NGCUC/EUC confluence and 110°W and time between arrival of potentially iron-enriched NGCUC waters at the equator and bloom inception. The velocity range is based on a range of estimated arrival times at the NGCUC/EUC confluence. Measured EUC velocity is the average for the 100-m-thick layer centered on the EUC core for the longitude and time range of interest. Insufficient ADCP data are available for the measured EUC velocity in 2005.

[31] Published measurements of iron in the EUC and model simulations of iron transfer across the Pacific in the EUC support the hypothesis that ENSO modulated variation in iron flux to the EUC can generate large-scale blooms along the equator. Model studies by *Wells et al.* [1999] indicate that relatively small increases (~ 2 nM) in iron concentrations of EUC source waters can fuel intense blooms along the equator. *Mackey et al.* [2002] present total dissolvable iron profiles from the equator between 150°E and 155°E that show variation greater than 2 nM. The highest concentrations (>5 nM) were observed near the peak of the 1997–1998 El Niño, and they were nearly double those observed during the 2000 La Niña. Assuming the same rate of loss during eastward transport, the amount upwelled in the east would be approximately twice as much when the waters reached the equatorial euphotic zone. This would significantly reduce iron limitation. Although sampling at different phases of the annual cycle may have influenced the observed differences in iron concentrations between the El Niño years (1993, 1997) and the La Niña year (2000), the observation of higher iron concentrations during both El Niño years suggests interannual modulation through ENSO variability in the western equatorial Pacific.

[32] The high-resolution ocean circulation model provided novel insight into dynamics of the NGCUC that in situ observations could not address. Cyclonic eddies along the northern New Guinea margin, predicted by the model, were validated with synoptic maps of the sea surface height anomaly. A coupled physical-biogeochemical model, including a sediment transport module, using the 12.5-km Pacific ROMS configuration is currently being developed. Additionally, higher resolution along the New Guinea margin, essential to accurately quantifying fluxes from the narrow New Guinea shelf, can be achieved with a nested modeling approach in which a higher-resolution domain over the NGCUC region is nested within the Pacific ROMS. This coupled model can be used to further investigate the hypothesis and quantify the impact of NGCUC circulation changes on large-scale equatorial Pacific biogeochemistry.

6. Conclusions and Implications

[33] Over the past decade satellites, moorings and ships have routinely observed the equatorial Pacific, allowing for the first time to link western Pacific circulation during El

Niño to large phytoplankton blooms in the central and eastern Pacific following El Niño. The area impacted by these blooms at their peaks was up to 4.8×10^5 km², equivalent to 171% of the entire coastal upwelling ecosystem off Peru (2.8×10^5 km² computed from 9-km climatological SeaWiFS chlorophyll concentrations; the criterion of chlorophyll concentrations >1 mg m⁻³ was used for estimates in both regions). We do not have in situ observations within these blooms to characterize consequences, however previous observations of responses to iron enrichment describe important changes in ecosystem productivity and food web interactions [*Martin et al.*, 1991; *Coale et al.*, 1996a, 1996b; *Behrenfeld et al.*, 1996; *Gordon et al.*, 1997; *Landry et al.*, 1997]. The blooms also represent biogeochemical perturbations at a scale that impacts global patterns of primary production [*Behrenfeld et al.*, 2001] and natural outgassing of carbon dioxide from the equatorial Pacific Ocean to the atmosphere [*Chavez et al.*, 1999]. Longer time series will be needed to determine if this phenomenon is persistent and influenced by multidecadal variability [*McPhaden and Zhang*, 2002; *Chavez et al.*, 2003].

[34] **Acknowledgments.** This work was supported by the Monterey Bay Aquarium Research Institute under the David and Lucile Packard Foundation (JPR, FPC), by NASA Oceanography program grant NAG5-10639 (JPR, PSP, FPC), by NASA grant NAG5-12392 (FPC), by the Ministry of Education, Culture, Sports, Science and Technology, Japan, under the TOCS project in JAMSTEC (IU), by Fundação de Amparo à Pesquisa do Estado de São Paulo through project JP 01/06921-3, and by the Instituto Oceanográfico da Universidade de São Paulo (PSP). The SeaWiFS Project (Code 970.2) and the Distributed Active Archive Center (Code 902) at the NASA Goddard Space Flight Center made possible the production and distribution, respectively, of SeaWiFS data; these activities are sponsored by NASA's Mission to Planet Earth Program. Processing and distribution of TOPEX/Poseidon and Jason-1 sea surface height observations were supported by the Physical Oceanography DAAC at NASA Jet Propulsion Laboratory. The ROMS research described in this paper was carried out, in part, at the Jet Propulsion Laboratory, California Institute of Technology, under contract with NASA. The ROMS computation was performed on the Columbia supercomputer managed by the NASA Ames Research Center. We thank the TAO Project Office, Michael J. McPhaden, Director, for provision of TAO buoy observations and P. Strutton for the empirical relationship used to quantify average euphotic depth in Figure 1.

References

- Barbeau, K., and J. W. Moffett (2000), Laboratory and field studies of colloidal iron oxide dissolution as mediated by phagotrophy and photolysis, *Limnol. Oceanogr.*, *45*, 827–835.
- Barber, R. T., and F. P. Chavez (1991), Regulation of primary productivity rate in the equatorial Pacific, *Limnol. Oceanogr.*, *36*, 1803–1815.

- Behrenfeld, M. J., A. J. Bale, Z. S. Kolber, J. Aiken, and P. G. Falkowski (1996), Confirmation of iron limitation of phytoplankton photosynthesis in the equatorial Pacific Ocean, *Nature*, **383**, 508–511.
- Behrenfeld, M. J., et al. (2001), Biospheric primary production during an ENSO transition, *Science*, **291**, 2594–2597.
- Chavez, F. P., and J. R. Toggweiler (1995), Physical estimates of global new production: The upwelling contribution, in *Upwelling in the Ocean: Modern Processes and Ancient Records*, edited by C. P. Summerhayes et al., pp. 313–320, John Wiley, Hoboken, N. J.
- Chavez, F. P., P. G. Strutton, G. E. Friederich, R. A. Feely, G. C. Feldman, D. G. Foley, and M. J. McPhaden (1999), Biological and chemical response of the equatorial Pacific Ocean to the 1997–98 El Niño, *Science*, **286**, 2126–2131.
- Chavez, F. P., J. Ryan, S. E. Lluch-Cota, and M. Niquen (2003), From anchovies to sardines and back: Multidecadal change in the Pacific Ocean, *Science*, **299**, 217–221.
- Coale, K. S., S. E. Fitzwater, R. M. Gordon, K. S. Johnson, and R. T. Barber (1996a), Control of community growth and export production by upwelled iron in the equatorial Pacific, *Nature*, **379**, 621–624.
- Coale, K. H., et al. (1996b), A massive phytoplankton bloom induced by an ecosystem-scale iron fertilization experiment in the equatorial Pacific Ocean, *Nature*, **383**, 495–501.
- Cresswell, G. R. (2000), Coastal currents of northern Papua New Guinea, and the Sepik River outflow, *Mar. Freshwater Res.*, **51**, 553–564.
- Fu, L.-L., E. J. Christiansen, C. A. Yamarone, M. Lefebvre, Y. Menard, M. Dorrer, and P. Escudier (1994), TOPEX/Poseidon mission overview, *J. Geophys. Res.*, **99**, 24,369–24,381.
- Gordon, R. M., K. H. Coale, and K. S. Johnson (1997), Iron distributions in the equatorial Pacific: Implications for new production, *Limnol. Oceanogr.*, **42**, 419–431.
- Hooker, S. B., W. E. Esaias, G. C. Feldman, W. W. Gregg, and C. R. McClain (1992), An overview of SeaWiFS and ocean color, *NASA Tech. Memo.*, *TM-104566*, vol. 1, 24 pp.
- Intergovernmental Panel on Climate Change (2001), *Climate Change 2001: The Scientific Basis. Contribution of Working Group I to the Third Assessment Report of the Intergovernmental Panel on Climate Change*, edited by J. T. Houghton et al., 881 pp., Cambridge Univ. Press, New York.
- Johnson, G. C., B. M. Sloyan, W. S. Kessler, and K. E. McTaggart (2002), Direct measurements of upper ocean currents and water properties across the tropical Pacific during the 1990s, *Prog. Oceanogr.*, **52**, 31–61.
- Johnson, K. S., K. H. Coale, V. A. Elrod, and N. W. Tindale (1994), Iron photochemistry in seawater from the equatorial Pacific, *Mar. Chem.*, **46**, 319–334.
- Johnson, K. S., R. M. Gordon, and K. H. Coale (1997), What controls dissolved iron concentrations in the world ocean?, *Mar. Chem.*, **57**, 137–161.
- Johnson, K. S., F. P. Chavez, and G. E. Friederich (1999), Continental-shelf sediment as a primary source of iron for coastal phytoplankton, *Nature*, **398**, 697–700.
- Kalnay, E., et al. (1996), The NCEP/NCAR 40-year reanalysis project, *Bull. Am. Meteorol. Soc.*, **77**, 437–471.
- Kineke, G. C., K. J. Wolfe, S. A. Kuehl, J. D. Milliman, T. M. Dellapenna, and R. G. Purdon (2000), Sediment export from the Sepik River, Papua New Guinea: Evidence for a divergent sediment plume, *Cont. Shelf Res.*, **20**, 2239–2266.
- Kuma, K., J. Tanaka, K. Matsunaga, and K. Matsunaga (2000), Effect of hydroxamate ferrisiderophore complex (ferrichrome) on iron uptake and growth of a coastal marine diatom, *Chaetoceros sociale*, *Limnol. Oceanogr.*, **45**, 1235–1244.
- Kuroda, Y. (2000), Variability of currents off the northern coast of New Guinea, *J. Oceanogr.*, **56**, 103–116.
- Landry, M. R., et al. (1997), Iron and grazing constraints on primary production in the central equatorial Pacific: An EqPac synthesis, *Limnol. Oceanogr.*, **42**, 405–418.
- Large, W. G., J. C. McWilliams, and S. C. Doney (1994), Oceanic vertical mixing: A review and a model with a nonlocal boundary layer parameterization, *Rev. Geophys.*, **32**, 363–403.
- Lindstrom, E. R., R. Lucas, R. Fine, E. Firing, S. Godfrey, G. Meyers, and M. Tsuchiya (1987), The Western Equatorial Pacific Ocean Study, *Nature*, **330**, 533–537.
- Mackey, D. J., J. E. O'Sullivan, and R. J. Watson (2002), Iron in the western Pacific: A riverine or hydrothermal source for iron in the Equatorial Undercurrent?, *Deep Sea Res., Part I*, **49**, 877–893.
- Martin, J. H., and R. M. Gordon (1988), Northeast Pacific iron distributions in relation to phytoplankton productivity, *Deep Sea Res.*, **35**, 177–196.
- Martin, J. H., R. M. Gordon, and S. E. Fitzwater (1991), The case for iron, *Limnol. Oceanogr.*, **36**, 1793–1802.
- Martin, J. H., et al. (1994), Testing the iron hypothesis in ecosystems of the equatorial Pacific Ocean, *Nature*, **371**, 123–129.
- McPhaden, M. J. (1999), Genesis and evolution of the 1997–98 El Niño, *Science*, **283**, 950–954.
- McPhaden, M. J., and D. Zhang (2002), Slowdown of the meridional overturning circulation in the upper Pacific Ocean, *Nature*, **415**, 603–608.
- McPhaden, M. J., et al. (1998), The Tropical Ocean–Global Atmosphere observing system: A decade of progress, *J. Geophys. Res.*, **103**, 14,169–14,240.
- Milliman, J. D., K. L. Farnsworth, and C. S. Albertin (1999), Flux and fate of fluvial sediments leaving large islands in the East Indies, *J. Sea Res.*, **41**, 97–107.
- Philander, S. G. (1990), *El Niño, La Niña and the Southern Oscillation*, 289 pp., Elsevier, New York.
- Polito, P. S., and O. T. Sato (2003), Patterns of sea surface height and heat storage associated to intraseasonal Rossby waves in the tropics, *J. Geophys. Res.*, **108**(C12), 3373, doi:10.1029/2002JC001684.
- Polito, P. S., O. T. Sato, and W. T. Liu (2000), Characterization and validation of the heat storage variability from TOPEX/Poseidon at four oceanographic sites, *J. Geophys. Res.*, **105**, 16,911–16,922.
- Ryan, J. P., P. S. Polito, P. G. Strutton, and F. P. Chavez (2002), Unusual large-scale blooms in the equatorial Pacific, *Prog. Oceanogr.*, **55**, 263–285.
- Shchepetkin, A. F., and J. C. McWilliams (2005), The regional oceanic modeling system (ROMS): A split-explicit, free-surface, topography-following-coordinate oceanic model, *Ocean Modell.*, **9**, 347–404.
- Sholkovitz, E. R., H. Elderfield, R. Szymczak, and K. Casey (1999), Island weathering: River sources of rare earth elements to the western Pacific Ocean, *Mar. Chem.*, **68**, 39–57.
- Smith, W. H. F., and P. Wessel (1990), Gridding with continuous curvature splines in tension, *Geophysics*, **55**, 293–305.
- Strutton, P. G., and F. P. Chavez (2000), Primary productivity in the equatorial Pacific during the 1997–1998 El Niño, *J. Geophys. Res.*, **105**, 26,089–26,101.
- Sunda, W. G. (2001), Bioavailability and bioaccumulation of iron in the sea, in *The Biogeochemistry of Iron in Seawater*, edited by D. R. Turner and K. A. Hunter, pp. 41–84, John Wiley, Hoboken, N. J.
- Tsuchiya, M., R. Lukas, R. A. Fine, E. Firing, and E. Lindstrom (1989), Source waters of the Pacific Equatorial Undercurrent, *Prog. Oceanogr.*, **23**, 101–147.
- Ueki, I., Y. Kashino, and Y. Kuroda (2003), Observation of current variations off the New Guinea coast including the 1997–1998 El Niño period and their relationship with Sverdrup transport, *J. Geophys. Res.*, **108**(C7), 3243, doi:10.1029/2002JC001611.
- Wells, M. L., G. K. Vallis, and E. A. Silver (1999), Tectonic processes in Papua New Guinea and past productivity in the eastern equatorial Pacific Ocean, *Nature*, **398**, 601–604.

Y. Chao and H. Zhang, Jet Propulsion Laboratory, California Institute of Technology, Pasadena, CA 91109, USA.

F. P. Chavez and J. P. Ryan, Monterey Bay Aquarium Research Institute, P.O. Box 628, 7700 Sandholdt Road, Moss Landing, CA 95039, USA. (ryjo@mbari.org)

P. S. Polito, Instituto Oceanográfico, Universidade de São Paulo, São Paulo 05508-120, Brazil.

I. Ueki, Japan Agency for Marine-Earth Science and Technology, 2-15 Natsushima-cho, Yokosuka, Kanagawa 237-0061, Japan.